

UNCLASSIFIED

Defense Technical Information Center
Compilation Part Notice

ADP011769

TITLE: Imaging of Photoexcited Carrier Distribution in Semiconductors by THz Beams

DISTRIBUTION: Approved for public release, distribution unlimited

This paper is part of the following report:

TITLE: International Conference on Terahertz Electronics [8th], Held in Darmstadt, Germany on 28-29 September 2000

To order the complete compilation report, use: ADA398789

The component part is provided here to allow users access to individually authored sections of proceedings, annals, symposia, etc. However, the component should be considered within the context of the overall compilation report and not as a stand-alone technical report.

The following component part numbers comprise the compilation report:

ADP011730 thru ADP011799

UNCLASSIFIED

Imaging of Photoexcited Carrier Distribution in Semiconductors by THz Beams

Masanori Hangyo, Masatsugu Yamashita, Yoshiaki Kitoh, Masayoshi Tonouchi

Abstract – A terahertz (THz) wave imaging system using photoconductive antennas as an emitter and detector has been constructed and the focussing characteristics of the beam near the sample position has been investigated. By using this system, the images of photoexcited carrier distribution in silicon have been obtained with spatial resolution of 2.5 mm by measuring the transmission of the focused THz beams.

I. INTRODUCTION

The transmittance and reflectance of electromagnetic waves in the microwave and infrared regions are much affected by free carriers in semiconductors [1,2]. Fig. 1 shows the transmittance of electromagnetic waves in the THz region calculated for 400- μm thick silicon wafers with various carrier densities. In this calculation, multiple reflection in the sample is neglected since we can exclude the multiple reflection by cutting off the multiply reflected electromagnetic waves in the time domain. The transmittance is greatly affected by the carrier density, especially in the low frequency region. By measuring the transmittance or reflectance, the density and mobility of the free carriers can be obtained without contact to the samples [1]-[3]. The free carriers are generated also by optical excitation and the transmittance and reflectance of the electromagnetic waves are affected by these photoexcited carriers. The change of the reflectance of microwaves by the irradiation of light has been used to characterise semiconductors [4,5]. Since the photoinduced reflectance is influenced by the dark resistivity, recombination time

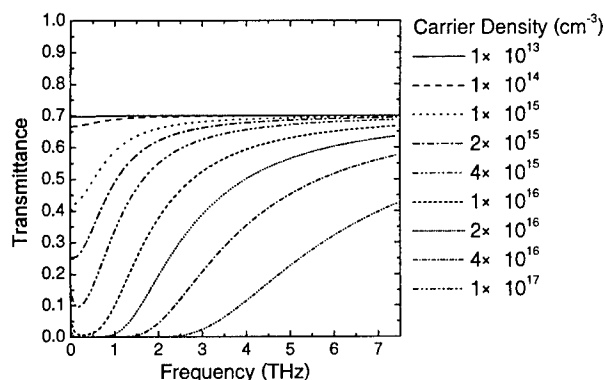


Fig. 1: Dependence of the transmittance of THz waves on the carrier density in silicon wafers

M. Hangyo, M. Yamashita, Y. Kitoh and M. Tonouchi are with the Research Center for Superconductor Photonics, Osaka University, 2-1 Yamadaoka, Suita, Osaka 565-0871, Japan

of photoexcited carriers, surface recombination velocity, and so on, versatile information on the free carriers and quality of the samples can be obtained.

Imaging of photoexcited carriers by using electromagnetic waves is important to evaluate the homogeneity of semiconductor samples. Recently, Nozokido *et al.* constructed a scanning near-field millimeter-wave microscope and applied it to visualising the photoexcited carrier distribution in silicon wafers and its time evolution with a spatial resolution of 110 μm [6]. In their system, the samples are placed very close to the tapered waveguide used as a probe. For introducing such noncontact evaluation systems in the fabrication process of semiconductor devices, it is preferable to separate samples and the probe widely. The imaging systems using THz waves are appropriate for this purpose [7].

In this paper, we constructed an imaging system using the focused THz beam generated and detected by photoconductive antennas and applied it to imaging the photoexcited carrier distribution in silicon wafers. The photoexcited carrier distribution is obtained with spatial resolution of ~ 2.5 mm.

II. THz IMAGING SYSTEM

Fig. 2 shows the schematic diagram of a THz imaging system. Optical pulses with a time width of ~ 80 fs, a wavelength of ~ 800 nm, and a repetition rate of 82 MHz from a mode-locked Ti:sapphire laser were used to excite a dipole-type photoconductive antenna on low-temperature grown GaAs (LT-GaAs) for generating THz wave pulses. The generated THz beam was focused on a sample by two paraboloidal mirrors (M_1 and M_2) and collected and focused by two paraboloidal mirrors (M_3 and M_4) into a dipole-type photoconductive antenna on LT-GaAs used as a detector. The focal length of M_1 and

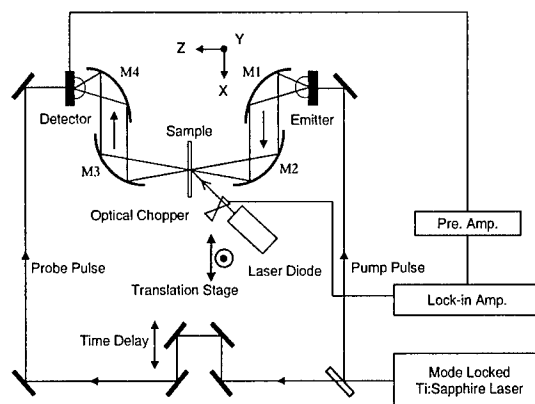


Fig. 2: Schematic diagram of the THz imaging system

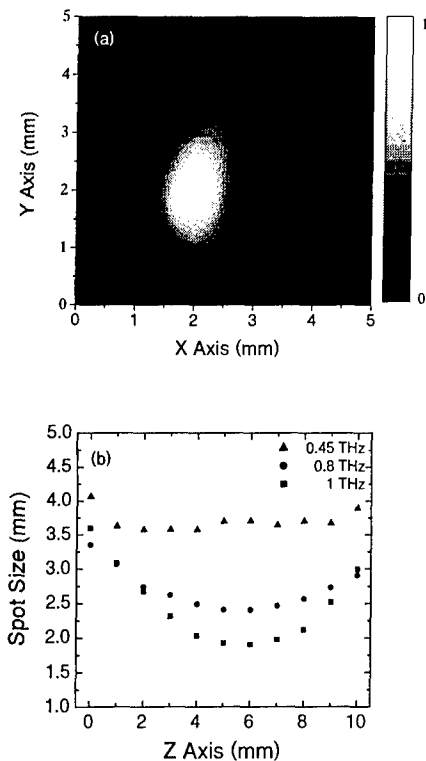


Fig. 3: (a) Maximum-amplitude distribution of THz waves in the X-Y plane at the focal point and (b) variation of the spot size along the beam direction at 0.45, 0.8 and 1 THz

M_4 was 7.6 cm and that of M_2 and M_3 was 11.9 cm. The detector was triggered by optical pulses divided from the exciting laser pulses after time delay.

The focusing characteristics of the THz beam near the focal point were measured by translating a metal mask with a pinhole of 1 mm diameter and taking a waveform in the time domain at each position. The exciting laser pulses were chopped at 2 kHz and the current induced by the THz electric field in the detector was lock-in detected. Fig. 3 (a) shows the distribution of the maximum amplitude of the waveform in the plane perpendicular to the beam direction at the focal point. The distribution is deformed from a simple Gaussian profile probably due to slight misalignment of optics. The full width at half maximum (FWHM) of the amplitude in the X and Y directions are 1.8 and 3.2 mm, respectively. Since the focussing characteristics are expected to be different for different frequencies, we calculated the Fourier spectrum of the waveform in the time domain at each position and fitted it with a Gaussian distribution function along the X axis at each frequency. The change of the FWHM of the amplitude thus obtained at 0.45, 0.8 and 1 THz along the Z axis (beam direction) is plotted in Fig. 3 (b). The FWHM at the focal point decreases with increasing frequency as expected from classical optics.

III. IMAGING OF PHOTOEXCITED CARRIERS

In order to see the effect of photoexcited carriers on the THz transmission for silicon wafers, the waveforms with and without CW laser diode illumination (800 nm, 100 mW) are measured. The silicon wafer is P-doped (2.5 Ω cm) and the thickness is 400 μ m. The diameter of the

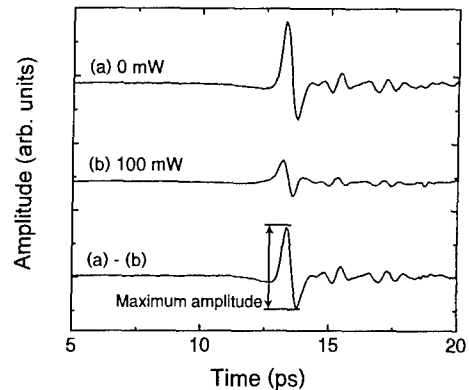


Fig. 4: Waveforms of the transmitted THz waves (a) without and (b) with CW laser diode illumination

laser spot on the sample is about 2 mm. Fig. 4 shows the waveforms (a) without and (b) with illumination of laser light. With the illumination of the laser light, the transmittance decreases due to the increase of the free carriers.

The position dependence of the THz transmission change is measured by translating the laser diode on an X-Y stage as shown in Fig. 2. Since the sample used is homogeneous, we are essentially measuring the position dependence of the THz transmission of the silicon wafer illuminated nonuniformly by the laser light. The CW light from the laser diode is chopped at 2 kHz instead of chopping the beam from the Ti:sapphire laser and the current induced by the THz electric field is lock-in detected. In this measurement, the photoinduced change of the THz waveform corresponding to (a) - (b) in Fig. 4 is measured.

The maximum-amplitude distribution of the waveforms in the X-Y plane at the focal point is shown in Fig. 5 (a). The FWHM's of the distribution are 3.9 mm for both X and Y axes. Since the spot size of the THz beam on the sample changes with frequency, the spatial resolution of the image of the photoexcited carriers will change with frequency. To confirm this, we Fourier transformed the waveform at each position and obtained the image at each frequency. The images at 300 GHz and 1.5 THz are shown in Figs. 5 (b) and (c), respectively. The FWHM's in the X and Y directions of the image at 300 GHz are 5.0 and 4.3 mm, respectively, and those at 1.5 THz are 3.6 and 3.5 mm, respectively. The spatial resolution increases with increasing frequency as expected [7].

Next, we show the dependence of the amplitude of the transmitted THz wave on the exciting laser intensity. Figs. 6 (a), (b) and (c) show the maximum-amplitude distribution for the exciting powers of 80, 160 and 250 mW, respectively. The amplitude increases with increasing the exciting laser power monotonically. Fig. 6 (d) shows the dependence of the amplitude on the exciting laser power. The amplitude increases linearly with increasing the laser power until \sim 150 mW and shows a trend of saturation with increasing the laser power further. This result indicates that the amplitude is proportional to the photoexcited carrier number when the exciting power is not too strong.

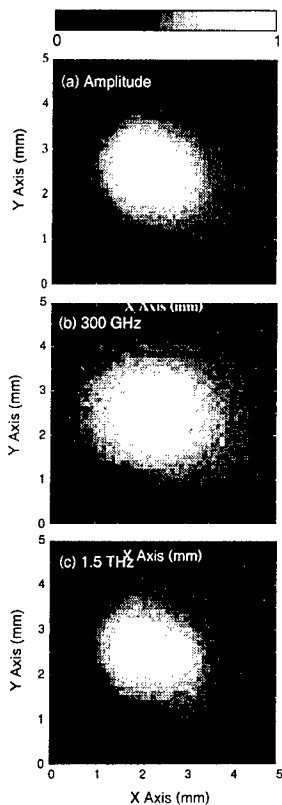


Fig. 5: Transmitted THz wave distribution for the silicon wafer illuminated by the laser diode corresponding to (a) the maximum amplitude, (b) the amplitude at 300 GHz and (c) the amplitude at 1.5 THz

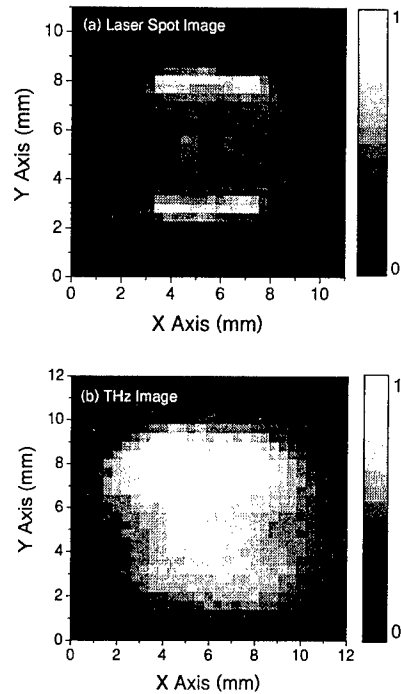


Fig. 7: (a) Distribution of the defocused exciting laser at the sample surface measured by the beam profiler and (b) its THz beam image

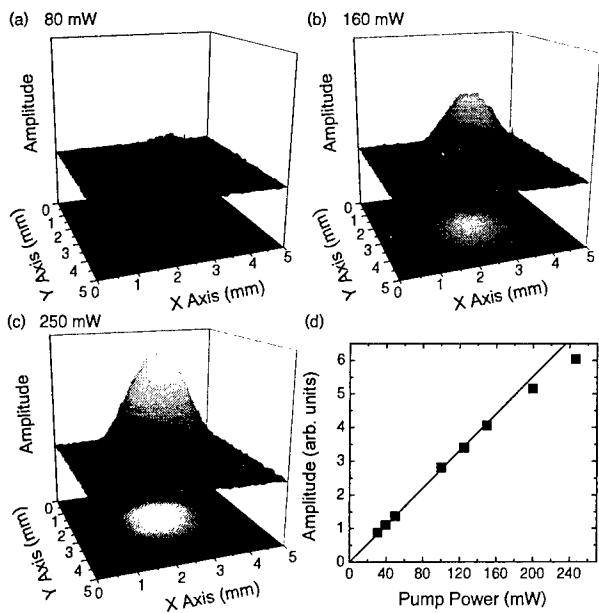


Fig. 6: Maximum-amplitude images of transmitted THz waves for (a) 80, (b) 160 and (c) 250 mW excitation, and (d) the dependence of the amplitude on the exciting laser power

Fig. 7 shows the THz image of the photoexcited carrier for the case of the defocused excitation of the laser diode. Fig. 7 (a) shows the laser intensity distribution at the sample measured with the beam profiler and Fig. 7 (b) shows the maximum-amplitude THz image of the

photoexcited carrier distribution corresponding to this defocused excitation condition. The intensity distribution of the defocused laser deviates from a Gaussian distribution considerably and this characteristic distribution is reflected in the THz maximum-amplitude image with decreased spatial resolution due to the THz beam spot size.

Since the photoexcited carrier distribution in silicon wafers depends on the chopping frequency of the exciting light due to the diffusion and recombination of the photoexcited carriers [8], the amplitude of the transmitted THz waves also changes with the chopping frequency. Fig. 8 (a) shows the change of the depth profile of the photoexcited carrier distribution in silicon with chopping frequency calculated assuming that the surface recombination velocity at the front surface can be neglected and the recombination time is 100 μ s.

The amplitude and penetration depth of the photoexcited carrier density oscillating with the chopping frequency decrease with increasing frequency. These changes of the distribution may cause the decrease of the THz amplitude with chopping frequency. Fig. 8 (b) shows the chopping frequency dependence of the THz amplitude. The amplitude decreases with increasing chopping frequency monotonically. Although the detailed calculation of the transmission of the THz wave is difficult because of the distribution of the photoexcited carriers, which causes the gradient of the complex refractive index in the sample, the amplitude may be approximately proportional to the total number of the photoexcited carrier oscillating with the chopping frequency. On this assumption, we calculate the frequency dependence of the amplitude and find that the

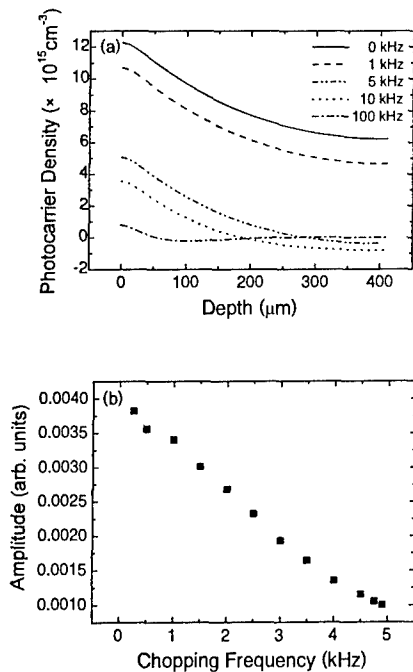


Fig. 8: (a) Calculated chopping frequency dependence of the photoexcited carrier distribution in silicon and (b) the measured chopping frequency dependence of the amplitude of the transmitted THz wave

result in Fig. 8 (b) is explained by assuming the recombination time to be $\sim 100 \mu\text{s}$.

IV. CONCLUSION

The THz wave imaging system using the photoconductive antennas as an emitter and detector is constructed. The beam waist at the sample is about 2.5 mm in our system, but it depends on frequency. The photoexcited carrier distribution in silicon wafers can be measured by using this imaging system with spatial

resolution of $\sim 2.5 \text{ mm}$. The THz imaging system in combination with photoexcitation will become an useful system for characterising semiconductor wafers under processing without electrical contact.

Acknowledgments

This work was partly supported by a Grant-in-aid for Scientific Research from the Ministry of Education, Science, Sports and Culture, Japan. This work was also partly supported by the public participation program for the promotion of creative info-communication technology R&D of Telecommunications Advanced Organization (TAO).

References

1. M. van Exter and D. Grischkowsky, "Carrier Dynamics of Electrons and Holes in Moderately Doped Silicon", *Phys. Rev. B*, Vol. 41, No. 17, pp. 12140-12149, 1990
2. T.-I. Jeon and D. Grischkowsky, "Characterization of Optically Dense, Doped Semiconductors by Reflection THz Time Domain Spectroscopy", *Appl. Phys. Lett.*, Vol. 23, No. 23, pp. 3032-3034, 1998
3. S. Nashima, O. Morikawa, K. Takata and M. Hangyo, "Temperature Dependence of Low Energy Carrier Dynamics of Silicon Studied by Terahertz Time Domain Spectroscopy", in this Proceedings
4. M. Kunst and G. Beck, "The Study of Charge Carrier Kinetics in Semiconductors by Microwave Conductivity Measurements", *J. Appl. Phys.*, Vol. 60, No. 10, pp. 3558-3566, 1986
5. M. Kunst and G. Beck, "The Study of Charge Carrier Kinetics in Semiconductors by Microwave Conductivity Measurements. II", *J. Appl. Phys.*, Vol. 63, No. 4, pp. 1093-1098, 1988
6. T. Nozokido, J. Bae and K. Mizuno, "Visualization of Photoexcited Free Carriers by Scanning Near-Field Millimeter-Wave Microscopy", *Appl. Phys. Lett.*, Vol. 77, No. 1, pp. 148-150, 2000
7. B. B. Hu and M. C. Nuss, "Imaging with Terahertz Waves", *Opt. Lett.*, Vol. 20, No. 16, pp. 1716-1718, 1995
8. S. M. Sze, *Physics of Semiconductor Devices*, 2nd ed., John Wiley & Sons, New York, 1981